Publisher: GSA
Journal: GEOL: Geology
DOI:10.1130/G36329.1

Self-organized pattern formation in coastal barrier washover deposits

Eli D. Lazarus* and Scott Armstrong

Environmental Dynamics Laboratory, School of Earth and Ocean Sciences, Cardiff University, Main Building, Park Place, Cardiff, CF10 3AT, UK

**E-mail address:* LazarusED@cf.ac.uk

ABSTRACT

Storm-driven overwash is a sediment-transport process fundamental to the evolution of low-lying coastal environments. Physical insight into overwash morphodynamics is crucial for improved risk assessment and hazard forecasting in vulnerable coastal zones. Spatially extended observations of washover deposits have shown that back-barrier shoreline planforms can be quasi-periodic. These rhythmic patterns have been attributed to the influence of a forcing template in bathymetry or topography, or inherent in the forcing itself. With an alternative to this prevailing explanation, we present results of a physical experiment and numerical model in which quasi-periodic patterns in washover deposits are self-organized, arising from interactions between barrier topography, routing of overwash flow, and sediment flux.

INTRODUCTION

Overwashing is a coastal physical process in which an elevated water level, typically a combined effect of tide, storm surge, wave set-up, and swash, crests a barrier beach and transports sediment landward, from the barrier front to the back-barrier environment, in a shallow overland flow. The sedimentary feature that forms as a result is a washover deposit. Essential to ecologically sensitive dune and marsh habitats (Seavey et al., 2011), overwashing enables barrier beaches and islands to maintain their height and width relative to rising sea level (FitzGerald et al., 2008). In extreme conditions, overwashing may escalate to inundation and inlet breaching. On developed barriers, overwashing constitutes a natural hazard. Although the majority of field, laboratory, and numerical-modeling investigations of overwash single out individual washover lobes or focus on a barrier's cross-shore profile (Donnelly et al., 2006; McCall et al., 2010; Williams et al., 2012; Lorenzo-Trueba and Ashton, 2014), some work has documented quasi-periodic patterns in washover deposits alongshore (Dolan, 1971; Dolan et al., 1979; Dolan and Hayden, 1981; Orford and Carter, 1984). These planform patterns (Figs. 1, DR1) have been attributed to forcing by trapped nearshore edge waves (Dolan et al., 1979; Orford and Carter, 1984), to the position and phase of sand-wave fields in the swash zone (Dolan, 1971), or explained as a function of pre-storm barrier topography (Stockdon et al., 2007; Houser et al., 2008).

We propose an alternative hypothesis: that alongshore quasi-periodicity in washover deposits may result from a process of self-organization rather than from a template in external forcing. A growing literature on rhythmic morphologies in coastal and terrestrial settings shows how patterns can self-organize in the absence of a pre-existing template, arising instead from feedbacks in coupled, nonlinear interactions between fluid flow and sediment transport (Werner, 1999). Self-organized pattern formation has been demonstrated in a variety of littoral and nearshore phenomena including beach cusps, bedforms and bars, alongshore spacing between rip currents, and regional-scale coastal planforms (Coco and Murray, 2007). Here, we extend spatial self-organization to overwash and washover. Results from a physical experiment and numerical model express spatial quasi-periodicity in washover deposits as a consequence of competition among topographic lows in the barrier (termed "throats") for cross-shore flow capture. Both models foster pattern formation in the absence of a forcing template. Dynamic redistribution of cross-shore flow along the barrier means that local morphological adjustments can have nonlocal effects elsewhere, affecting back-barrier planform morphometry overall.

PHYSICAL MODEL

To generate spatial patterns of washover in a simple physical model, we constructed a countertop "tub flume," starting with a 50 L plastic tub (605 × 370 × 200 mm). We removed a 600 × 70 mm panel from one side and attached a level 600 × 300 mm particleboard platform inscribed with a 20 mm grid (Fig. DR2). For each trial, we laid down on the platform a barrier (600 × 40 × 10 mm) of dry-sieved sand (200–500 μm), with its leading edge 5 mm outboard of the tub lip. We then slowly filled the tub with a garden hose at a flow rate ~100 mL s^{-1}. The hose was fixed to the base of the tub opposite the platform to minimize water-surface disturbance. Kitchen scour pads at both sides of the tub gap dampened edge effects.

We define the long dimension of the barrier facing the tub as the "seaward" side, and the side facing the platform as the "back-barrier." During a trial, the water level in the tub rose to the height of the barrier before cresting somewhere along its length, flowing across the barrier top, incising the back-barrier edge, and forming an initial erosional throat. Sediment entrained by this "overwashing" flow was deposited on the platform as an incipient washover lobe. A succession of washover lobes followed. As the washover lobes adjusted their slopes to the imposed condition of cross-shore uniform flow, sediment transport eventually ceased; a trial ended once the back-barrier shoreline stopped transgressing and maintained a steady-state morphology (for a berm 10 mm high, typically after 30 s). Because of the relatively slow infill rate and the barrier's wide aspect ratio, the barrier never overwashed in a single event spanning its full length. We photographed trials using an overhead-mounted SLR camera in multi-shoot mode (~2.5 frames s^{-1}), orthorectified the photographs using the pre-inscribed platform grid as reference points, and extracted back-barrier shoreline position using a digitized grid with 5 mm spacing.

NUMERICAL MODEL

To expand upon the physical experiment, we developed a simplified cellular numerical model of an erodible barrier atop a level plane. Although other, fully hydrodynamic models are capable of resolving overwash processes in four dimensions for generalized or spatially explicit domains (Cañizares and Irish, 2008; Roelvink et al., 2009), our exploratory approach tests whether a comparatively limited set of processes is sufficient to produce quasi-periodic back-barrier patterns analytically comparable to those observed in the field and in our laboratory trials.

Like in the physical experiment, we start with a level, square-lattice domain of I x J rows and columns (cells of arbitrary unit length; i,j notation indicates alongshore, cross-shore position). Along the left edge we superimpose an erodible barrier one column wide, with an initial height $Z_{i,1} = Z_b = 1$. The driving force in this model is water height (H) against the barrier's seaward side. At time $t = 0$, water and barrier heights are equal ($H = Z_b = 1$). To initiate cross-shore flow, two perturbations are incised in the barrier at random locations alongshore. Incision depth is $d_i = bA_{i,1:2}$, where $A_{i,1:2}$ is the difference in elevation between the first and second rows of cells alongshore, and b is a constant proportion of the barrier height, such that $d_i << Z_b$.

Water against the barrier is treated as a conserved quantity. Water height along the barrier is adjusted at each time step to account for volumetric loss to cross-shore discharge:

$$H(t) = H_o - (Z_{bo} - Z_b)/I \quad (1)$$

where H_o is initial water height and Z_{bo} is initial barrier height. Flow across the barrier occurs where water height exceeds barrier height. Discharge (q_w) at a given local minimum in the barrier is scaled by the proportion (p) of cells in the alongshore dimension nearer to that minimum than to other minima (McNamara and Werner, 2008):

$$q_{w\,i,1} = p_i(H_i - Z_{b\,i}) \quad (2)$$

The amount of flow through a given throat in the barrier thus depends on its alongshore location relative to other throats.

Water flux past the barrier is distributed proportionally from a given cell to its nearest downslope neighbors, and sediment flux from a cell is calculated as a proportion of water flux $q_{si,j} = cq_{wi,j}$, where c is a constant $0 < c < 1$. We prevent sediment flux up positive slopes. We also include a threshold parameter q_{wmin} that sets the minimum water depth required to move sediment from a given cell. Model topography evolves as flow propagates across the back-barrier surface. Flow stops when there is insufficient water depth to advance down slope; a topographic contour ($Z = \alpha$) representing back-barrier shoreline position is then recorded. In both the physical experiment and numerical model, all water flux into the back-barrier domain drains out. Our results therefore do not account explicitly for overwash flow ponding into a body of standing water (Shaw et al., 2015).

At the beginning of each model time step, we allow the domain to diffuse in the alongshore dimension, with a periodic boundary condition, according to

$$\dot{Z}(t) = K\frac{\partial^2 Z}{\partial Y^2} \quad (3)$$

where Y is the alongshore unit length of a cell ($Y = 1$) and K is a diffusivity coefficient ($0 \leq K < 1$). Diffusive smoothing is not essential to the dynamics of the model, but $K > 0$ functionally represents two assumptions: first, that the erodible barrier substrate is non-cohesive, well rounded, and not reinforced by vegetation, such that any steep slopes will tend to relax; and second, that oblique or lateral flow into the throats from atop the barrier contributes to the gradual shoaling and widening of an incision's initially sharp relief.

To determine the alongshore location of a new barrier incision in the next time step, the model calculates a normalized hydraulic gradient along the face of the barrier according to

$$\hat{\varepsilon}(t) = \frac{\varepsilon(t)}{\max(\varepsilon(t))}, \text{ where } \varepsilon(t) = \sum_{i=1}^{i=\mathrm{I}} A_{i,1:2}\frac{(Z_{bi} - H_i)}{2\,\pi\,T}\ln\left(\frac{R}{r_i}\right) \quad (4)$$

where T (units L T^{-1}) is transmissivity, R (units L) is the radius of influence, r (units L) is distance from the topographic low, and A is the difference in elevation between the first and second rows of cells at a given alongshore position. Where $\hat{\varepsilon}(t)$ exhibits a unique global maximum, a new incision will occur at that barrier cell. Otherwise, a location is selected at random from among equal maxima. Motivated by the Thiem solution (Thiem, 1906) to steady-state radial flow to a pumping well, this formulation treats throats along a barrier like an array of wells in an aquifer. We make the conceptual assumption that a throat, like a well, draws from water pushed against the barrier within the limits of some

DOI:10.1130/G36329.1

lateral radius of influence. Much as wells in close proximity have collective drawdown effects, we assume that neighboring throats with overlapping radii of influence likewise depress the hydraulic gradient between them, inhibiting the formation of a new incision there. (We do not use the normalized alongshore hydraulic gradient to adjust the volume of cross-shore flow, only to site new incisions.) Although the A term introduces some dependence on back-barrier topography (i.e., incision becomes more likely where the back-barrier face is steepest, and less likely where a widening washover lobe has filled in behind the barrier), the alongshore hydraulic gradient tends to seed new incisions near the midpoint of the longest undissected barrier section intact at a given time step. Because in the physical experiment new washover lobes appeared intermittently, the numerical model includes a 50% probability at each time step that a new incision will occur. But, as with the diffusivity term, the model dynamics do not depend on this rule. Alongshore spacing between throats is determined by ephemeral local maxima in $\hat{\varepsilon}(t)$, not by an imposed parameter.

RESULTS AND DISCUSSION

We use wavelet analysis to quantify spectral power in the back-barrier shoreline planform over a range of spatial scales (Lazarus et al., 2011). Wavelet analysis convolves a scaled filter (wavelet) with a data series (here, the detrended back-barrier shoreline) to produce a transform of local signal power at that spatial scale. Squaring the scaled transform yields a measure of signal variance (Fig. DR3), and calculating the mean variance at each scale produces a power spectrum. We provide further explanation in the Data Repository.

In the physical experiment, localized overwashing along the barrier results in a quasi-periodic series of washover lobes (manifest in repeated trials). A typical sequence of pattern development is shown in Figure 2 (A–E). After an initial phase of rapid growth, lobe width and amplitude slow and stabilize, and some lobes may go dormant as new lobes appear. Uninterrupted back-barrier segments are eventually tapped by small lobes that weld onto the flanks of larger neighbors. The power spectra (Fig. 3, A–E) for the sequence in Fig. 2 (A–E) show a wavelength (~100 mm) that becomes increasingly well defined, with a wandering but persistent secondary local maximum (~30–40 mm).

Figure 2 (F–J) shows a back-barrier sequence from the numerical model, with spectral features (Fig. 3, F–J) similar to those in the physical experiment. In the numerical model, new overwash slows growth at existing lobes by capturing flow. Alongshore emplacement of new lobes becomes increasingly controlled by the situation of existing lobes. The exemplars in Figs. 2 and 3 demonstrate the numerical model's capacity to reproduce the kind of shapes and pattern spectra generated in the physical experiment, but the model is not limited to these spectra. We matched the domain size and initial barrier height in the model to those in the experiment, but did not tune the dynamics of the former to replicate the latter. An exploration of the model's parameter space produces quasi-periodic back-barrier patterns with a wide range of dominant and ancillary wavelengths (Figs. DR4–DR7).

When the stochastic elements of the model are held constant across trials, parameter sensitivity tests (Fig. DR4) indicate that the spectral signature is most sensitive to adjustment of the diffusivity coefficient (K), followed by the minimum water depth for entrainment (q_{wmin}), sediment proportion (c), and the radius of influence (R). All else being equal, diffusivity exerts a strong control on lobe wavelength, with high diffusivity resulting in long wavelengths (water height exceeds barrier elevation in more locations alongshore), and vice versa. Diffusivity also drives a kind of backwater effect (Chow, 1959): if diffusion moves more sediment into a throat than the overwashing flow can export, that localized shoaling changes the hydraulic potential along the barrier, increasing the likelihood that washover will initiate (or reactivate) elsewhere. Otherwise, minimum water depth and the sediment-entrainment proportion also affect lobe amplitude because lobe size increases with sediment supply (a high minimum water-depth threshold or a low sediment-entrainment proportion result in blunted lobes). The effect of the radius of influence is strongest early in a simulation. A large radius forces any new incision farther away from an existing throat (and therefore closer to the midpoint between two throats), and new throats are separated by the longest segments of undisturbed barrier in the first few time steps. Finally, while the stochastic “coin-flip” rule governing incision at a given time step does not change how the model works, the time interval between successive washover lobes can affect the spectral signature of the back-barrier shoreline (Fig. DR5). Early lobes grow larger the longer they persist before a new throat impinges upon their water supply. The larger they grow, the more they prohibit new throats from incising near them. Moreover, under constant forcing, flow through established throats lowers water height, thus limiting discharge through later throats and, by extension, the size of their washover lobes.

The ensemble mean and median of the power spectra in Fig. DR4 indicate a dominant wavelength (~100 mm) similar to that in the physical experiment, but this result derives from the matched aspect ratios of the barriers’ low height relative to their extended length dimension. Additional modeling suggests that the difference between barrier height and the surface elevation behind the barrier (back-barrier slope) may be a key control on washover spacing. Increasing the barrier height (and commensurate water level) in the numerical model increases the dominant wavelength of washover (Fig. DR6). Because we treat initial incision depth as a proportion of barrier height, initial incisions in tall barrier are deeper, and a taller barrier has more sand available for washover. Furthermore, lateral diffusion of a deeper incision affects a greater reach of the barrier top, which contributes more sediment to washover, lengthens the cumulative local radius of influence around the throat, and suppresses initiation of new throats nearby.

Water level elevated relative to a low, erodible barrier drives the morphodynamics in both our experiment and model. Our system designs do not explicitly include wave action. In the storm-impact scale for barrier islands by Sallenger (2000), a barrier enters the “overwash regime” if the summed elevation of wave run-up height (swash height plus wave set-up), storm surge, and tidal height is high enough to overtop the barrier and initiate cross-shore flow. The essential parameter of the impact scale is relative height, not breaking-wave dynamics. Therefore, we suggest that our application of an elevated water level effectively includes wave-driven contributions to overwash and washover deposition as a cumulative, time-averaged effect of barrier overtopping. Given that flow not only crests but fully crosses the barrier top in our models, our results may be most representative of extreme storm impacts in the continuum between the “overwash” and “inundation” regimes (Sallenger, 2000).

Because the initial topography of our modeled berms is featureless, the spatial patterns that form do so as a function of flow routing and associated sediment transport.

Self-organized pattern formation typically involves a positive feedback that grows without bound unless a negative feedback arrests it. Here, a single washover lobe will grow until its slope adjusts to the paired condition of uniform flow and lateral diffusion, or until a new overwash throat claims some of the flow. An idealized barrier perturbed with simultaneous, equidistant, equal-sized throats produces washover lobes that draw the same proportion of available water, grow at the same rate, and shut off at the same time, but the equidistant perturbation of the same size is an unstable state; a barrier perturbed at random locations with throats incised to random depths still goes to a fixed wavelength (Fig. DR7).

According to the typology described in the review of experimental geomorphology by Paola et al. (2009), the results of our tub experiment and numerical model demonstrate external, kinematic similarity to natural systems, but, like many morphodynamic experiments, they do not satisfy the conditions of force comparability necessary for dynamical scaling. However, at the coarser scales of interest (e.g., the growth of washover lobes and rearrangement of the back-barrier shoreline at a dominant alongshore wavelength), the dynamics of our models are insensitive to fine-scale behavior (e.g., granular or cell-to-cell interactions), which suggests scale independence (Werner, 1999). The fact that our models are not dynamically scaled versions of natural examples does not detract from their utility (Paola et al., 2009). Rather, the apparent scale independence in our results might help frame opportunities to advance physical insight (Coco and Murray, 2007) into scaling behavior in overwashing and in breaching morphodynamics more broadly, perhaps through a generic Froude modeling approach (Paola et al., 2009). Detailed stratigraphic analysis of washover deposits in the field, combined with time-series measurements of onshore forcing conditions, also offer a way forward (Shaw et al., 2015), and, if extended alongshore over significant distances, could reveal spatio-temporal washover patterns of a storm's wax and wane – details otherwise invisible even in high-resolution remote sensing of pre-storm and post-storm topography.

CONCLUSIONS

Our results do not necessarily refute template-based explanations for storm-driven morphological changes along coastal barriers, but do complicate them by demonstrating that antecedent topography may not be reflected in the post-storm back-barrier planform. We offer that quasi-periodicity in back-barrier planforms can arise as a consequence of self-organized overwash flow rather than a pre-existing template in barrier topography or onshore forcing. Competition among barrier throats for capture of overwash flow means that morphological change at one throat has nonlocal effects on washover deposition elsewhere along the barrier, even under constant forcing. Overwash therefore may behave like other self-organized coastal phenomena, whereby coupled feedbacks between flow and topography, rather than flow or topography alone, dictate how the morphology evolves. A spatially extended, coupled-process perspective is therefore crucial for improved vulnerability assessment and storm-impact forecasting in coastal zones.

ACKNOWLEDGMENTS

We are grateful for discussions with D. McNamara and C. Paola, and we thank J. Shaw, D. Mohrig, and an anonymous referee for constructive reviews. The British Society for Geomorphology and Cardiff University's Master in Earth Science program provided funding for this work.

REFERENCES CITED

Cañizares, R., and Irish, J.L., 2008, Simulation of storm-induced barrier island morphodynamics and flooding: Coastal Engineering, v. 55, p. 1089–1101, doi:10.1016/j.coastaleng.2008.04.006.

Chow, V. T., 1959, Open Channel Hydraulics: New York, McGraw Hill, 680 p.

Coco, G., and Murray, A.B., 2007, Patterns in the sand: From forcing templates to self-organization: Geomorphology, v. 91, p. 271–290, doi:10.1016/j.geomorph.2007.04.023.

Dolan, R., 1971, Coastal landforms: Crescentic and rhythmic: Geological Society of America Bulletin, v. 82, p. 177–180, doi:10.1130/0016-7606(1971)82[177:CLCAR]2.0.CO;2.

Dolan, R., and Hayden, B., 1981, Storms and shoreline configuration, Journal of Sedimentary Petrology, v. 51, p. 737–744.

Dolan, R., Hayden, B., and Felder, W., 1979, Shoreline periodicities and edge waves: The Journal of Geology, v. 87, p. 175–185, doi:10.1086/628407.

Donnelly, C., Kraus, N., and Larson, M., 2006, State of knowledge on measurement and modeling of coastal overwash: Journal of Coastal Research, v. 22, p. 965–991, doi:10.2112/04-0431.1.

FitzGerald, D.M., Fenster, M.S., Argow, B.A., and Buynevich, I.V., 2008, Coastal impacts due to sea-level rise: Annual Review of Earth and Planetary Sciences, v. 36, p. 601–647, doi:10.1146/annurev.earth.35.031306.140139.

Houser, C., Hapke, C., and Hamilton, S., 2008, Controls on coastal dune morphology, shoreline erosion and barrier island response to extreme storms: Geomorphology, v. 100, p. 223–240, doi:10.1016/j.geomorph.2007.12.007.

Lazarus, E., Ashton, A., Murray, A.B., Tebbens, S., and Burroughs, S., 2011, Cumulative versus transient shoreline change: dependencies on temporal and spatial scale: Journal of Geophysical Research Earth Surface, v. 116, F02014.

Lorenzo-Trueba, J., and Ashton, A.D., 2014, Rollover, drowning, and discontinuous retreat: distinct modes of barrier response to sea-level rise arising from a simple morphodynamic model: Journal of Geophysical Research. Earth Surface, v. 119, p. 779–801, doi:10.1002/2013JF002941.

McCall, R.T., Van Thiel de Vries, J.S.M., Plant, N.G., Van Dongeren, A.R., Roelvink, J.A., Thompson, D.M., and Reniers, A.J.H.M., 2010, Two-dimensional time dependent hurricane overwash and erosion modeling at Santa Rosa Island: Coastal Engineering, v. 57, p. 668–683, doi:10.1016/j.coastaleng.2010.02.006.

McNamara, D.E., and Werner, B.T., 2008, Coupled barrier island–resort model: 2. Tests and predictions along Ocean City and Assateague Island National Seashore, Maryland: Journal of Geophysical Research Earth Surface, v. 113, F01017.

Orford, J.D., and Carter, R.W.G., 1984, Mechanisms to account for the longshore spacing of overwash throats on a coarse clastic barrier in southeast Ireland: Marine Geology, v. 56, p. 207–226, doi:10.1016/0025-3227(84)90014-8.

Paola, C., Straub, K., Mohrig, D., and Reinhardt, L., 2009, The “unreasonable effectiveness” of stratigraphic and geomorphic experiments: Earth-Science Reviews, v. 97, p. 1–43, doi:10.1016/j.earscirev.2009.05.003.

Roelvink, D., Reniers, A., van Dongeren, A.P., van Thiel de Vries, J., McCall, R., and Lescinski, J., 2009, Modelling storm impacts on beaches, dunes and barrier islands: Coastal Engineering, v. 56, p. 1133–1152, doi:10.1016/j.coastaleng.2009.08.006.

Sallenger, A.H., 2000, Storm impact scale for barrier islands: Journal of Coastal Research, v. 16, no. 3, p. 890–895.

Seavey, J.R., Gilmer, B., and McGarigal, K.M., 2011, Effect of sea-level rise on piping plover Charadrius melodus breeding habitat: Biological Conservation, v. 144, p. 393–401, doi:10.1016/j.biocon.2010.09.017.

Shaw, J., You, Y., Mohrig, D., and Kocurek, G., 2015, Tracking hurricane-generated storm surge with washover fan stratigraphy: Geology, doi: 10.1130/G36460.1.

Stockdon, H.F., Sallenger, A.H., Jr., Holman, R.A., and Howd, P.A., 2007, A simple model for the spatially-variable coastal response to hurricanes: Marine Geology, v. 238, p. 1–20, doi:10.1016/j.margeo.2006.11.004.

Thiem, G., 1906, Hydrologic methods: Leipzig, J.M. Gebhardt, 56 p.

Werner, B.T., 1999, Complexity in natural landform patterns: Science, v. 284, p. 102–104, doi:10.1126/science.284.5411.102.

Williams, J.J., Buscombe, D., Masselink, G., Turner, I.L., and Swinkels, C., 2012, Barrier Dynamics Experiment (BARDEX): Aims, design and procedures: Coastal Engineering, v. 63, p. 3–12, doi:10.1016/j.coastaleng.2011.12.009.

FIGURE CAPTIONS

Figure 1. Washover lobes on Cape Hatteras National Seashore, North Carolina, USA, (A) near Buxton, following the 1962 Ash Wednesday storm, and (B) near Avon, in 1972. Black arrows indicate direction of overwash transport. Washover periodicity is quantified in Fig. DR1. Photos by the (A) U.S. Army and (B) National Park Service, in the public domain via the U.S. Geological Survey Photographic Library.

Publisher: GSA
Journal: GEOL: Geology
DOI:10.1130/G36329.1

Figure 2. Exemplar back-barrier shoreline sequences from the physical experiment (A–E) and the numerical model (F–J), rotated a quarter turn anticlockwise relative to the row/column orientation in the model description. Bold line indicates shoreline position at that time step; finer lines in each box show position at previous time steps. Arrows indicate flow direction. Parameters for numerical output shown: $I = J = 114$ (5 mm cells match experimental grid measurements); $K = 0.35$, $c = 0.23$, $R = 20$ mm, $q_{wmin} = 0.0295$ mm, $\alpha = 0.0295$ mm, $b = 0.1$, $T = 1$.

Figure 3. Log-log power spectra, calculated as mean wavelet-transform variance at spatial scales from 20 to 280 mm (base 2), for the experimental (A–E) and modeled (F–J) back-barrier shoreline planforms shown in the corresponding panels of Fig. 2. Filled circles indicate spectrum at the time step noted; finer lines show spectra at previous time steps. Both sequences illustrate the development of a dominant wavelength (~100 mm) and ancillary peaks or saddles.

[1]GSA Data Repository item 2015xxx, xxxxxxxx, is available online at www.geosociety.org/pubs/ft2015.htm, or on request from editing@geosociety.org or Documents Secretary, GSA, P.O. Box 9140, Boulder, CO 80301, USA.

GSA DATA REPOSITORY

Supplementary Figures & Captions (DR1–DR7)

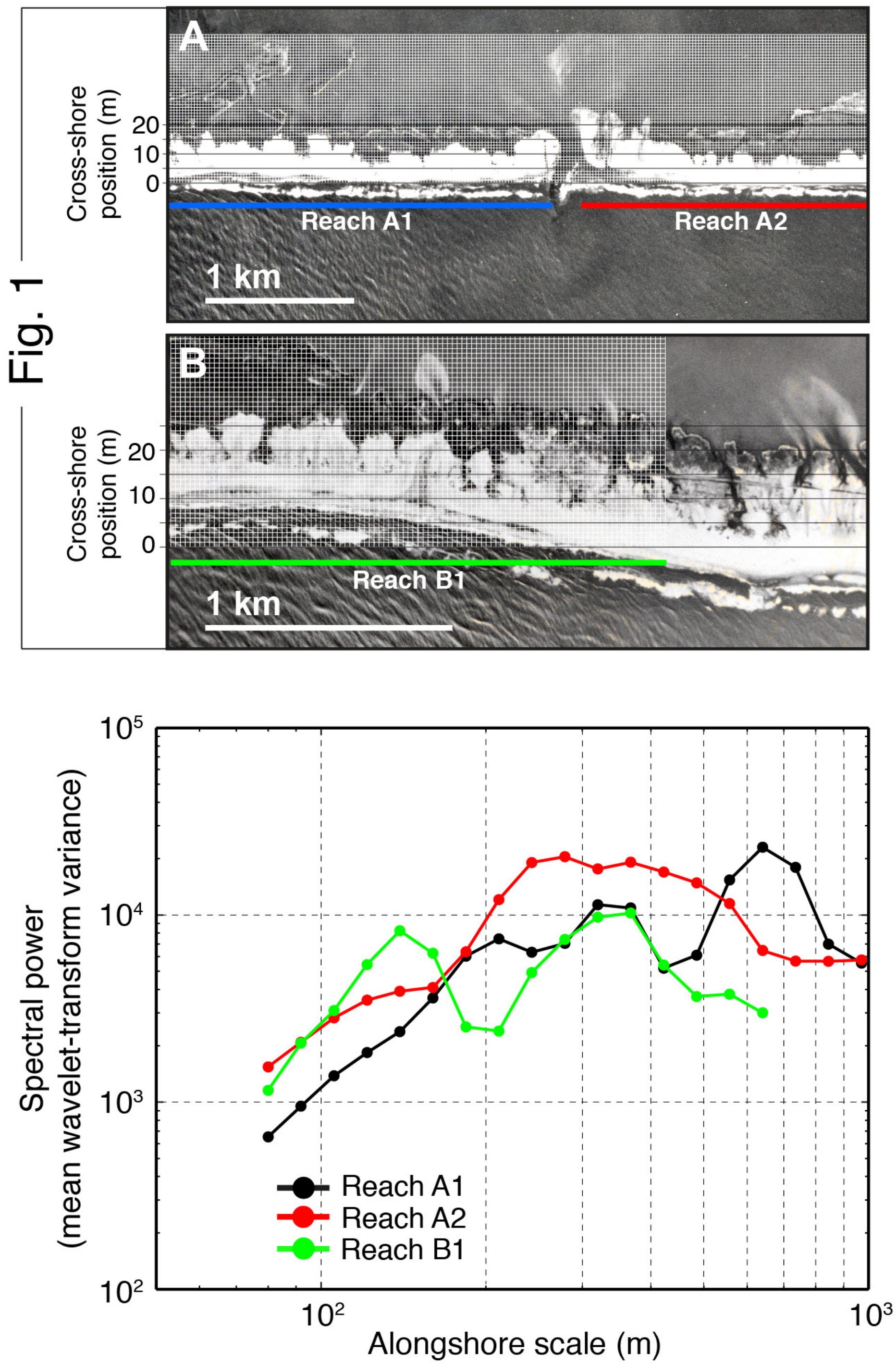

Figure DR1. To calculate the power spectra of the washover shown in Fig. 1, we superimposed square-lattice grids scaled to both photos, respectively, such that each grid square = ~20 m. We did not measure across the inlet evident in Fig. 1A.

Likewise, we measured only the first two-thirds of the barrier in Fig. 1B, up to where the washover planform becomes indistinct. Wavelet analysis of the resulting back-barrier shorelines (detrended) returns a dominant alongshore wavelength for Reach A1 ~600 m, a secondary peak ~350 m, and a tertiary saddle ~200 m. For Reach A2, a dominant wavelength is less pronounced (in agreement with the photograph), with roughly equivalent power across ~250–450 m wavelengths. Reach B1 appears bimodal, with a peak ~150 m and another ~300–350 m, consistent with where adjacent smaller-scale lobes have begun to merge.

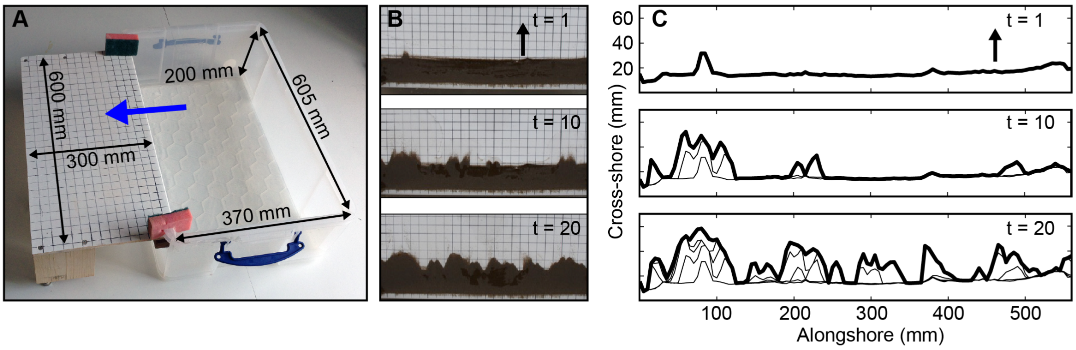

Figure DR2. (A) "Tub flume" apparatus used for the physical experiment. Blue arrow indicates flow direction. **(B)** Photo sequence showing plan-view changes in the experimental barrier during an experimental trial. **(C)** Superimposed, digitized back-barrier planforms extracted from orthorectified versions of the raw photos in B. Bold line marks back-barrier planform at time step shown. Black arrows in B and C indicate flow direction.

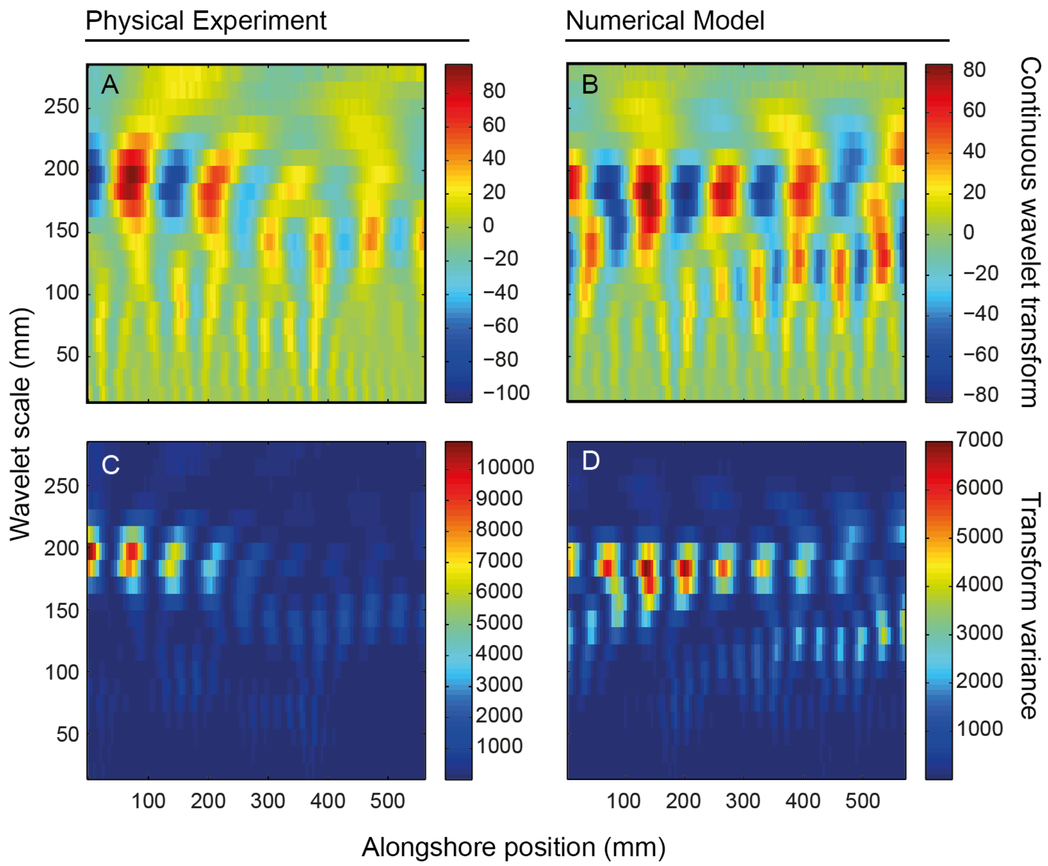

Figure DR3. A wavelet can walk along the signal in discrete steps, like a caliper, or slide continuously between consecutive points. We use the latter, called a continuous wavelet transform. Despite its sampling redundancy, a continuous transform can reveal spatial heterogeneities in the data in greater detail. Squaring the scaled wavelet transform yields a measure of signal variance. Calculating the mean variance at each scale produces a power spectrum much like a Fourier analysis. Using both the averaged power spectrum (Fig. 3) and the full wavelet transform (above) allows both a coarse summary and detailed quantitative description of patterns, often spatially localized, embedded in the data series. In this analysis we apply a Morlet wavelet,

$$\psi(f(x)) = \left(e^{-(f(x))^2/2}\right)\cos\,(5f(x))$$

a common waveform whose shape is conducive to resolving mesoscale features in a data series, where ψ is the wavelet transform and $f(x)$ is back-barrier shoreline position (detrended). To minimize edge effects at the beginning and end of the original signal, we reflect the signal several times, convolve the extended signal, and then use an interior multiple of the transform. As a further precaution against edge effects, we also only consider spatial scales smaller than half the length of the data series. This figure shows continuous wavelet transforms for **(A)** the experimental and **(B)** numerical back-barrier planforms shown in Fig. 2E and Fig. 2J, respectively. Panels **(C)** and **(D)** show transform variance (the squares of the values plotted in A and B). Mean transform variance calculated at each wavelet scale yields the power spectra shown in Figs. 3E and 3J.

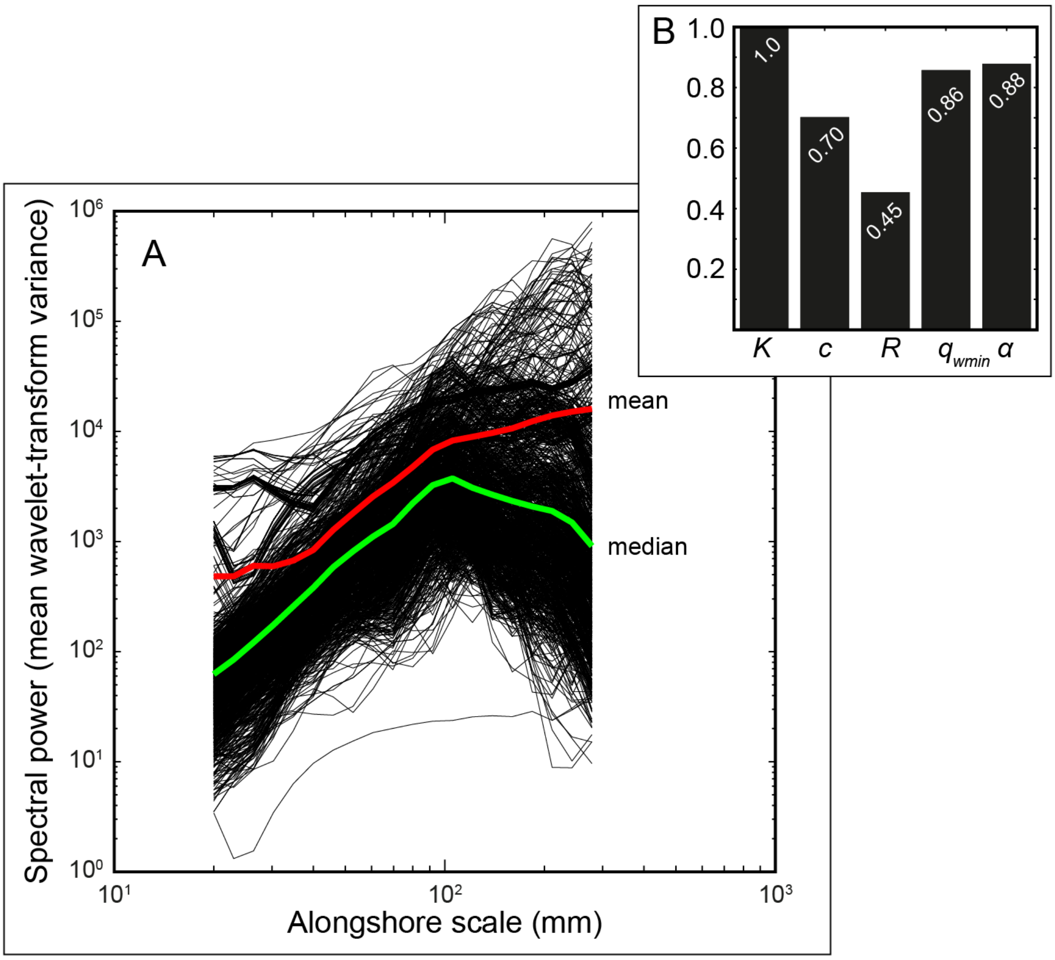

Figure DR4. (A) Power spectra at time step $t = 25$ for 9600 combinations of model parameters tested over the following intervals: diffusivity, $K = 0{:}0.1{:}0.9$; sediment-entrainment proportion, $c = 0.1{:}0.1{:}0.4$; radius of influence, $R = 10{:}10{:}50$; minimum water depth, $q_{wmin} = 0{:}0.01{:}0.05$; and topographic contour $\alpha = 0.01{:}0.01{:}0.08$. The same stochastic sequences were used for each model run. Incision-depth proportion ($b = 0.1$) and transmissivity ($T = 1$ L T^{-1}) were held constant throughout. The ensemble mean and median spectra are plotted in red and green, respectively. The ensemble median spectrum (green) captures a dominant wavelength ~100 mm. **(B)** Normalized standard deviation in the power spectra resulting from varying each parameter in turn.

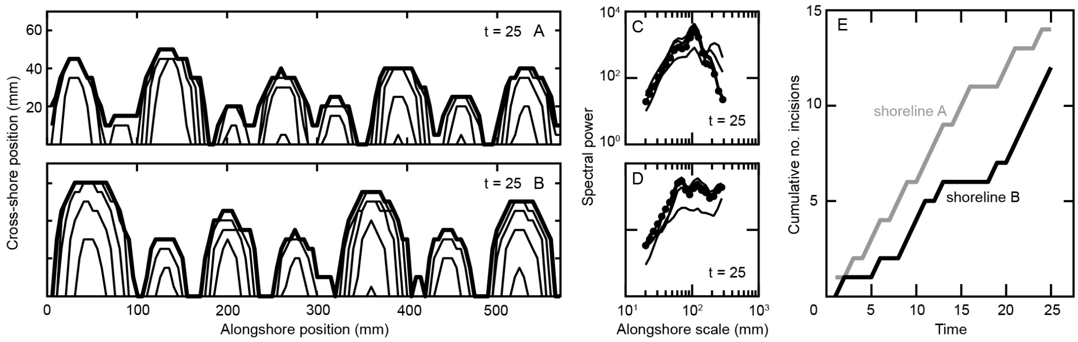

Figure DR5. Relative timing of washover emplacement during a storm event can affect the spectral signature of the back-barrier planform. Although the same parameter settings (see Fig. 2) were used to generate the planforms in **(A)** (same as Panel J in Fig. 2) and **(B)**, the randomized sequence in which new washover lobes were initiated differed between the two trials, resulting in unimodal **(C)** and bimodal **(D)** power spectra, respectively. The cumulative number of incisions over time in sequences A and B are shown in **(E)**. Fewer early-stage washover lobes may foster spectrum modes > 1, while a more continuous emplacement regime results in a strongly unimodal spectrum.

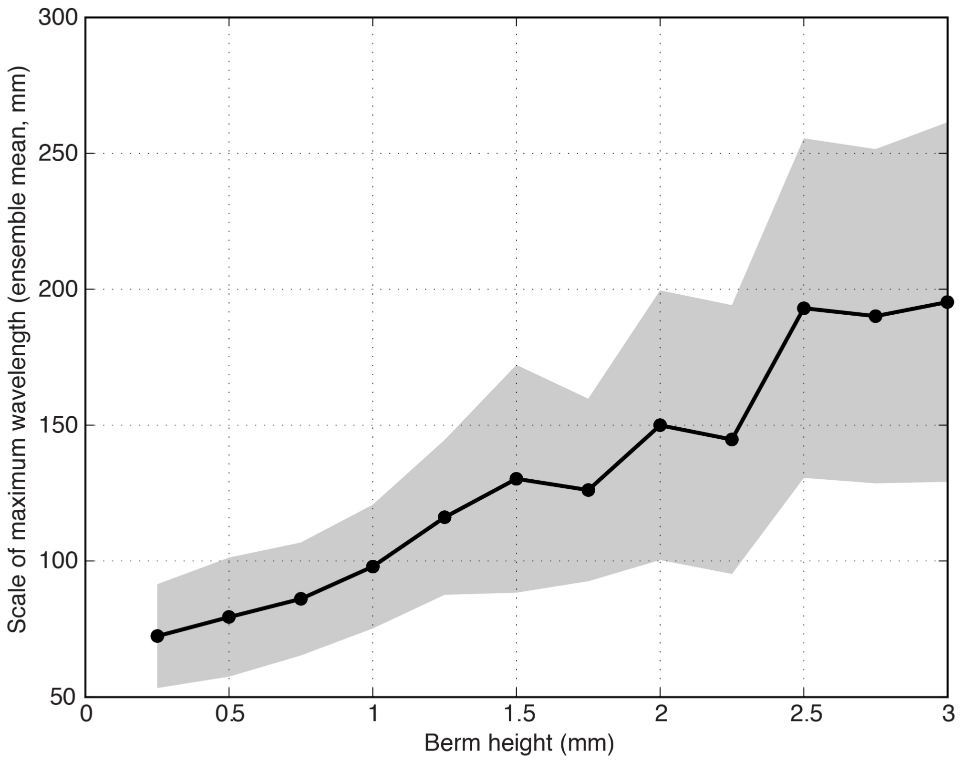

Figure DR6. Holding other dimensions in the numerical model held constant, changing barrier (berm) height exerts a strong, consistent control on dominant washover wavelength. This figure shows the mean scale of maximum wavelength (with gray envelope denoting ± 1SD around the mean) increasing with barrier height (Z_b). For a given height, the mean maximum wavelength is calculated from an ensemble of 30 trials with the same parameter settings but different stochastic sequences. Here, $I = J = 140$ (~5 mm cells), $K = 0.3$, $c = 0.25$; $R = 20$; $q_{wmin} = 0.02$; $\alpha = 0.02$ mm, $b = 0.2$, $T = 1$.

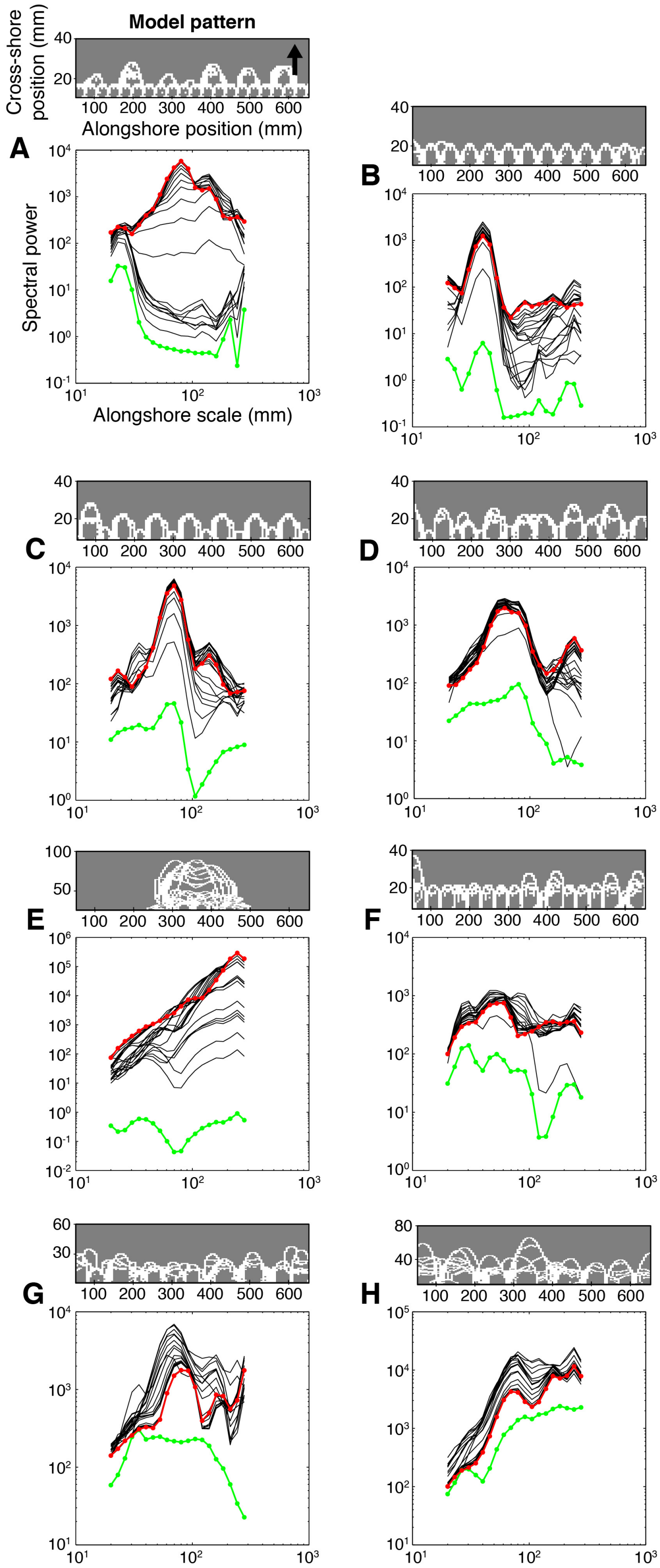

Figure DR7. This figure illustrates further exploration of self-organized washover behavior in the numerical model. Gray boxes showing back-barrier shorelines (white), where flow direction is bottom to top (black arrow), correspond to power spectra immediately below, where the spectrum at $t = 1$ is in green and the final spectrum at $t = 30$ is in red (finer lines represent spectra at intermediate time steps). For the results shown, parameter settings are: $I = J = 140$ (~5 mm cells), $K = 0.3$, $c = 0.25$; $R = 20$; $q_{wmin} = 0.02$; $\alpha = 0.02$ mm, $b = 0.2$, $T = 1$, $Z_b = 1$. The same stochastic sequence is used for all trials. **(A)** The barrier is perturbed with an initial-condition ($t = 0$) "template" of equidistant incisions of equal depth at a spacing of 6 cells (~30 mm). In this case, the 30 mm template controls washover spacing for nearly half the trial, but the dense spacing breaks down when subtle differences in the alongshore hydraulic gradient begin to trigger new incisions, destabilizing the template-driven pattern and creating a new dominant wavelength (~70 mm). **(B)** The initial-condition ($t = 0$) template of equidistant, equal-depth incisions is set to 10 cell (~50 mm) and **(C)** 17 cell (~85 mm) spacing; in each case the template persists as the dominant washover wavelength. **(D)** When the barrier at $t = 0$ is perturbed at 15 random locations alongshore with incisions of equal depth, the barrier still adjusts to a dominant wavelength. **(E)** If initially perturbed at $t = 0$ with a single, large incision (8 cells wide to 80% the height of the barrier), the barrier demonstrates a runaway positive feedback: the initial throat is so large that no other incisions can compete for flow, and a single washover lobe dominates the back-barrier. **(F)** The barrier at $t = 0$ is perturbed every 7 cells alongshore (~35 mm) with incisions of random depths between 0–60% of the barrier height, again finding a final spectrum that differs from the initial condition. **(G)** and **(H)** show back-barrier patterns that evolve under two different stochastic sequences, respectively, for which the initial barrier is perturbed at 20 random locations alongshore with incisions of random depths between 0–60% of the barrier height.